

March 1, 2021

TO: Distribution

FROM: Shantanu P. Naidu, Steven R. Chesley, Davide Farnocchia
Solar System Dynamics Group (392R), Jet Propulsion Laboratory,
California Institute of Technology

SUBJECT: Updated orbit of Dimorphos, the satellite of binary near-Earth asteroid
(65803) Didymos.

This IOM is an update to IOM 392R-20-001, in which we used mutual event times observed in lightcurve data obtained between 2003 and 2019 to estimate three possible solutions for the orbit of Didymos' satellite, now named Dimorphos. In this IOM, we document an improvement in the data treatment and modeling of the observables, and use new data obtained between December 2020 and January 2021 to refine the estimate of the orbit. The new data consist of 12 observations and allow us to rule out two of the three previous solutions and reduce the uncertainties of the remaining solution. The formal 3σ orbital phase uncertainty of the current solution during the planned Double Asteroid Redirection Test (DART) mission impact in October 2022 is about 6.6° , which satisfies the mission requirement 55 days prior to the DART impact.

1 Methods

Our orbital estimation method is described in IOM 392R-20-001, however we made some modifications to the technique used for measuring and modeling contact times as described below.

1.1 Improvements to the data treatment

We measured mutual event times in observations from 2003, 2015, 2017, 2019, and 2020/2021 using an improved technique that allowed us to reduce measurement bias and uncertainty. In IOM 392R-20-001, we measured $T_{1.5}$ as the mid-point between T_1 and T_2 and $T_{3.5}$ as the mid-point between T_3 and T_4 . This approach introduces errors when there are overlapping occultations and eclipses or when there are partial events, such that only a fraction of the satellite occults/eclipses the primary or gets occulted/eclipsed by the primary. Overlapping events have ill-defined T_2 and T_3 whereas partial events lack T_2 and T_3 . A more robust technique is to measure $T_{1.5}$ and $T_{3.5}$ as the times when the drop in brightness of the system is half of the total drop in brightness due to a full secondary event. For the Didymos system, with a diameter ratio (secondary/primary) of 0.21, a full secondary event causes a drop in brightness of 4.2% (Pravec et al., 2006), so $T_{1.5}$ and $T_{3.5}$

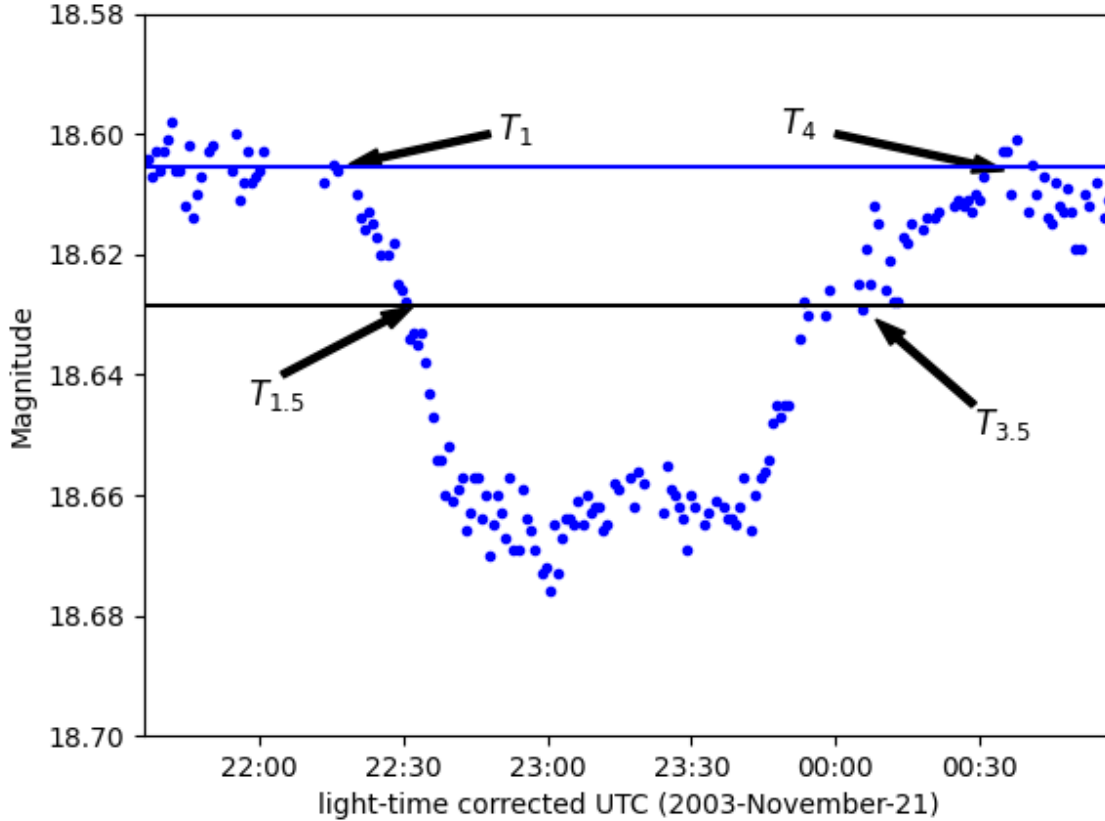


Figure 1: A secondary eclipse event showing various contact times. The horizontal blue line represents the baseline magnitude of the system and is computed by taking the average magnitude of the points just outside the mutual event. The black line indicates a magnitude that is higher than the baseline by 0.023 mag, which represents a 2.1% drop in brightness of the system.

are measured as the times when the brightness drops by 2.1%, which corresponds to a magnitude increase of 0.023. Figure 1 shows the contact times for a secondary eclipse event from 2003. We assigned 1σ uncertainties of $(T_{1.5} - T_1)/2$ and $(T_4 - T_{3.5})/2$ to $T_{1.5}$ and $T_{3.5}$, respectively. Table 1 lists all the observations.

Table 1: Mutual event times measured in observations from 2003, 2015, 2017, 2019, 2020, and 2021. All times are one-way light-time corrected to reflect the time of the events at the asteroid, not the times that they were observed at Earth.

Calendar date (UTC)	Julian date	Contact	Occulted/Eclipsed object	Event type	1σ Uncertainty (days)
2003 Nov 20 22:48:00	2452964.4500	1.5	Secondary	Eclipse	0.004
2003 Nov 21 00:01:26	2452964.5010	3.5	Secondary	Eclipse	0.003
2003 Nov 21 22:31:00	2452965.4382	1.5	Secondary	Eclipse	0.006

2003 Nov 21 23:52:30	2452965.4948	3.5	Secondary	Eclipse	0.011
2003 Nov 22 04:32:35	2452965.6893	1.5	Primary	Eclipse	0.004
2003 Nov 22 05:50:21	2452965.7433	3.5	Primary	Eclipse	0.004
2003 Nov 23 04:19:46	2452966.6804	1.5	Primary	Eclipse	0.004
2003 Nov 23 05:38:49	2452966.7353	3.5	Primary	Eclipse	0.003
2003 Nov 24 04:03:12	2452967.6689	1.5	Primary	Eclipse	0.003
2003 Nov 24 05:26:52	2452967.7270	3.5	Primary	Eclipse	0.007
2003 Nov 26 03:40:36	2452969.6532	1.5	Primary	Eclipse	0.004
2003 Nov 26 05:03:33	2452969.7108	3.5	Primary	Eclipse	0.003
2003 Nov 27 21:27:12	2452971.3939	1.5	Secondary	Eclipse	0.005
2003 Nov 29 21:01:17	2452973.3759	1.5	Secondary	Eclipse	0.003
2003 Nov 30 02:57:33	2452973.6233	1.5	Primary	Eclipse	0.003
2003 Dec 02 03:55:35	2452975.6636	3.5	Primary	Occultation	0.005
2003 Dec 03 03:38:44	2452976.6519	3.5	Primary	Occultation	0.011
2003 Dec 03 08:16:13	2452976.8446	1.5	Secondary	Eclipse	0.007
2003 Dec 03 09:46:22	2452976.9072	3.5	Secondary	Occultation	0.009
2003 Dec 04 02:17:31	2452977.5955	1.5	Primary	Eclipse	0.005
2003 Dec 04 03:35:59	2452977.6500	3.5	Primary	Occultation	0.005
2003 Dec 18 23:29:19	2452992.4787	1.5	Primary	Eclipse	0.013
2003 Dec 19 00:50:58	2452992.5354	3.5	Primary	Occultation	0.009
2003 Dec 19 05:23:16	2452992.7245	1.5	Secondary	Eclipse	0.009
2003 Dec 19 06:44:55	2452992.7812	3.5	Secondary	Occultation	0.008
2003 Dec 20 05:19:06	2452993.7216	1.5	Secondary	Eclipse	0.004
2003 Dec 20 06:32:15	2452993.7724	3.5	Secondary	Occultation	0.008
2015 Apr 13 04:54:20	2457125.7044	3.5	Primary	Occultation	0.007
2015 Apr 14 09:25:37	2457126.8928	1.5	Secondary	Eclipse	0.004
2017 Feb 25 03:50:06	2457809.6598	1.5	Primary	Occultation	0.006
2017 Feb 25 05:45:10	2457809.7397	3.5	Primary	Eclipse	0.007
2017 Apr 18 07:46:16	2457861.8238	1.5	Primary	Eclipse	0.003
2017 May 04 06:49:32	2457877.7844	3.5	Primary	Occultation	0.005
2019 Jan 31 08:39:24	2458514.8607	3.5	Secondary	Eclipse	0.007
2019 Jan 31 13:03:21	2458515.0440	1.5	Primary	Occultation	0.005
2019 Mar 09 01:42:31	2458551.5712	1.5	Secondary	Occultation	0.007
2019 Mar 09 02:35:13	2458551.6078	3.5	Secondary	Eclipse	0.005
2019 Mar 10 02:15:47	2458552.5943	3.5	Secondary	Eclipse	0.006
2019 Mar 11 02:15:30	2458553.5941	3.5	Secondary	Eclipse	0.005
2020 Dec 17 08:50:38	2459200.8685	1.5	Secondary	Eclipse	0.006
2020 Dec 17 09:36:43	2459200.9005	3.5	Secondary	Eclipse	0.007
2020 Dec 23 08:32:55	2459206.8562	3.5	Secondary	Eclipse	0.007
2020 Dec 23 12:35:42	2459207.0248	1.5	Primary	Occultation	0.006
2020 Dec 23 13:04:47	2459207.0450	3.5	Primary	Occultation	0.007
2021 Jan 08 10:57:12	2459222.9564	1.5	Primary	Eclipse	0.005
2021 Jan 08 11:35:39	2459222.9831	3.5	Primary	Eclipse	0.006
2021 Jan 09 10:50:26	2459223.9517	1.5	Primary	Eclipse	0.010
2021 Jan 09 11:21:15	2459223.9731	3.5	Primary	Eclipse	0.010

2021 Jan 10 11:11:02	2459224.9660	3.5	Primary	Eclipse	0.007
2021 Jan 14 09:56:44	2459228.9144	1.5	Primary	Eclipse	0.005
2021 Jan 14 10:26:41	2459228.9352	3.5	Primary	Eclipse	0.009

1.2 Improvements to the model

We made some improvements to the model used in IOM 392R-20-001 for calculating the contact times, $T_{1.5}$ and $T_{3.5}$, of occultations and eclipses. In the previous model we assumed that occultations and eclipses would be visible in lightcurves for their entire durations. This assumption holds when the Sun-target-observer phase angle is zero. However at non-zero phase angles, eclipses and occultations will be observable for shorter durations: eclipses will be observable only when a shadow is cast on the part of the target’s surface that is visible from Earth, while occultations will be observable only when the sunlit part of the target’s surface is occulted. We took these phase effects into account in the updated model.

For primary events, we computed the point on the surface of the primary that is being eclipsed or occulted by the secondary, which is assumed to be a point. We then use the SPICE geometry finder (Acton et al., 2018) to calculate intervals when the eclipsed point is visible from the Earth or when this occulted point is sunlit. The beginnings and ends of these intervals are taken to be the computed values of $T_{1.5}$ and $T_{3.5}$.

There are similar phase effects for secondary events. The dark part of the surface of the secondary does not contribute to the lightcurves. The only portion of the secondary surface that contributes to the lightcurves is the area that is sunlit and oriented towards Earth. So, for secondary events, the measured $T_{1.5}$ represents the instant when half of this visible area goes into an eclipse/occultation and $T_{3.5}$ represents the instant when half of the visible area comes out of an eclipse/occultation. In the previous model we introduced an error in the computed times by assuming that these contact times correspond to the instants when the center of figure of the secondary disc went into/came out of an eclipse/occultation. We reduced this error by computing the separation between the center of figure and the center of the visible area of the secondary and multiplying this separation by the relative velocity of the secondary in the direction of the separation.

We changed the SPICE aberration corrections from ‘LT’ to ‘CN’ and ‘XLT’ to ‘XCN’. The ‘CN’ and ‘XCN’ light-time corrections are done iteratively until convergence is achieved and have higher precision than the ‘LT’ and ‘XLT’ options, which use only one iteration.

Figures 2 and 3 compare the solutions and formal 3σ uncertainties estimated using the old and new methods corresponding to solution 1 in IOM 392R-20-001. The nominal values of both solutions are very similar, however the uncertainties of the new solution are about 75% of the old one. This improvement can be attributed to the smaller measurement uncertainty and modeling errors in the new method.

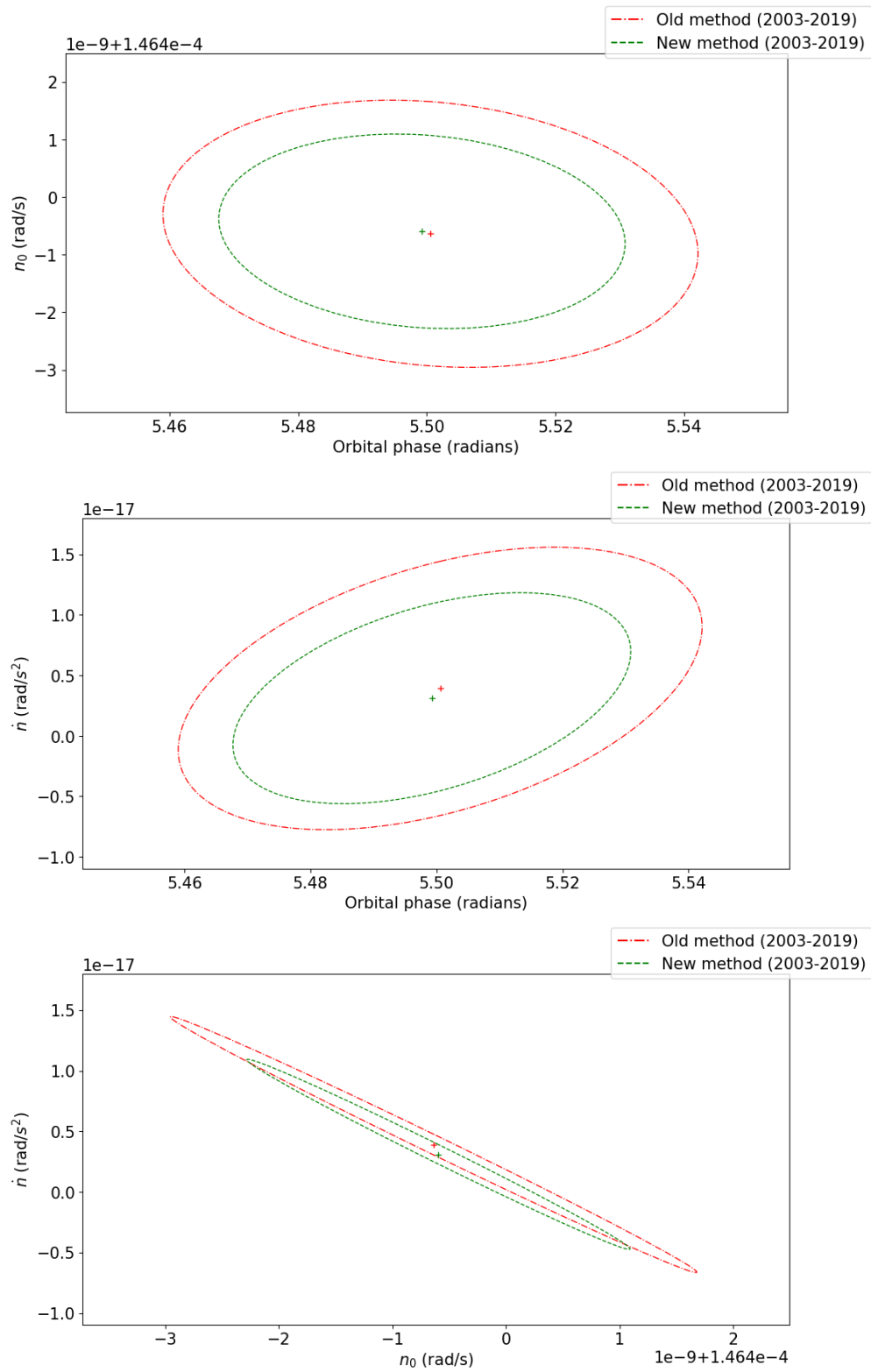


Figure 2: Projections of the best-fit parameters and their 3σ uncertainties estimated using the old (red) and the new (green) methods. Solutions are at epoch 2003-Nov-20.0 TDB.

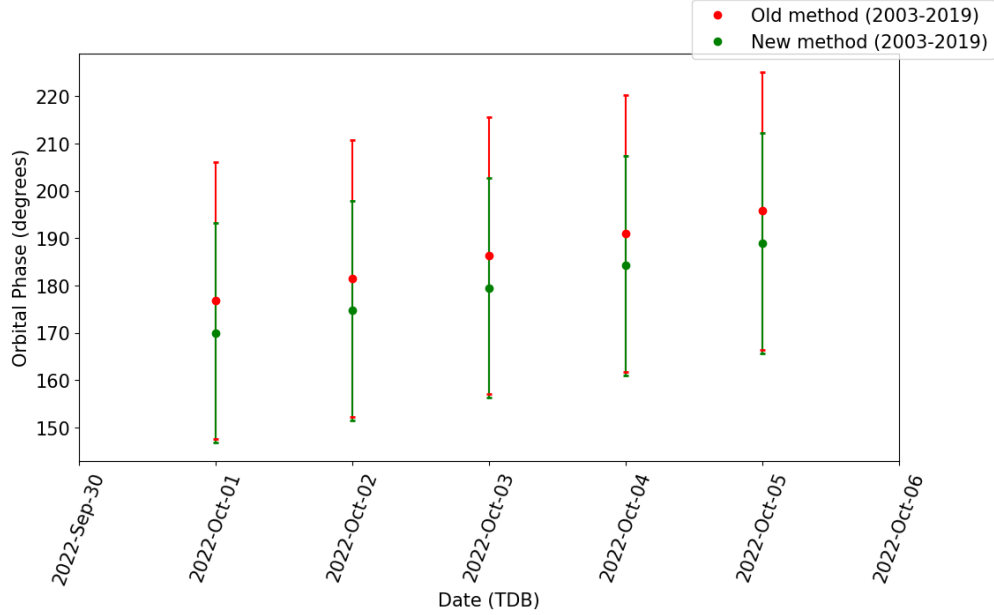


Figure 3: Predicted orbital phase and formal 3σ uncertainties during the planned DART impact using the old (red) and the new (green) methods.

2 Results

2.1 Effect of 2020-2021 lightcurves

We extracted 12 data points from the lightcurves observed in 2020 December and 2021 January. Figures 4, 5, and 6 show projections of the best-fit parameters and their covariances for the three solutions from IOM 392R-20-001 as we incrementally added data from 2020 and 2021 to the fits. Solution 1 stays within its 1σ uncertainty region as new data is added, however solutions 2 and 3 move outside their 3σ confidence interval, which suggests that only solution 1 can generate reliable predictions, whereas solutions 2 and 3 are incompatible with the full dataset. The χ^2 of solution 1 is 51.8, which is significantly lower than that of solutions 2 and 3, which have χ^2 of 105.8 and 98.3, respectively. Therefore, we can now rule out solutions 2 and 3.

In Figures 4, 5, and 6, as well as elsewhere in this memo, orbital phase is the angle in the orbital plane measured from the 0° longitude in the ECLIPJ2000 frame, as opposed to mean anomaly, which is measured from the ascending node. Both angles are measured in the direction of the orbital motion of the satellite.

2.2 Orbit pole

We estimated the mutual orbit pole by performing orbit fits for various pole orientations starting with the best-fit parameters of solution 1. Figure 7 shows χ^2 as a function of mutual orbit pole

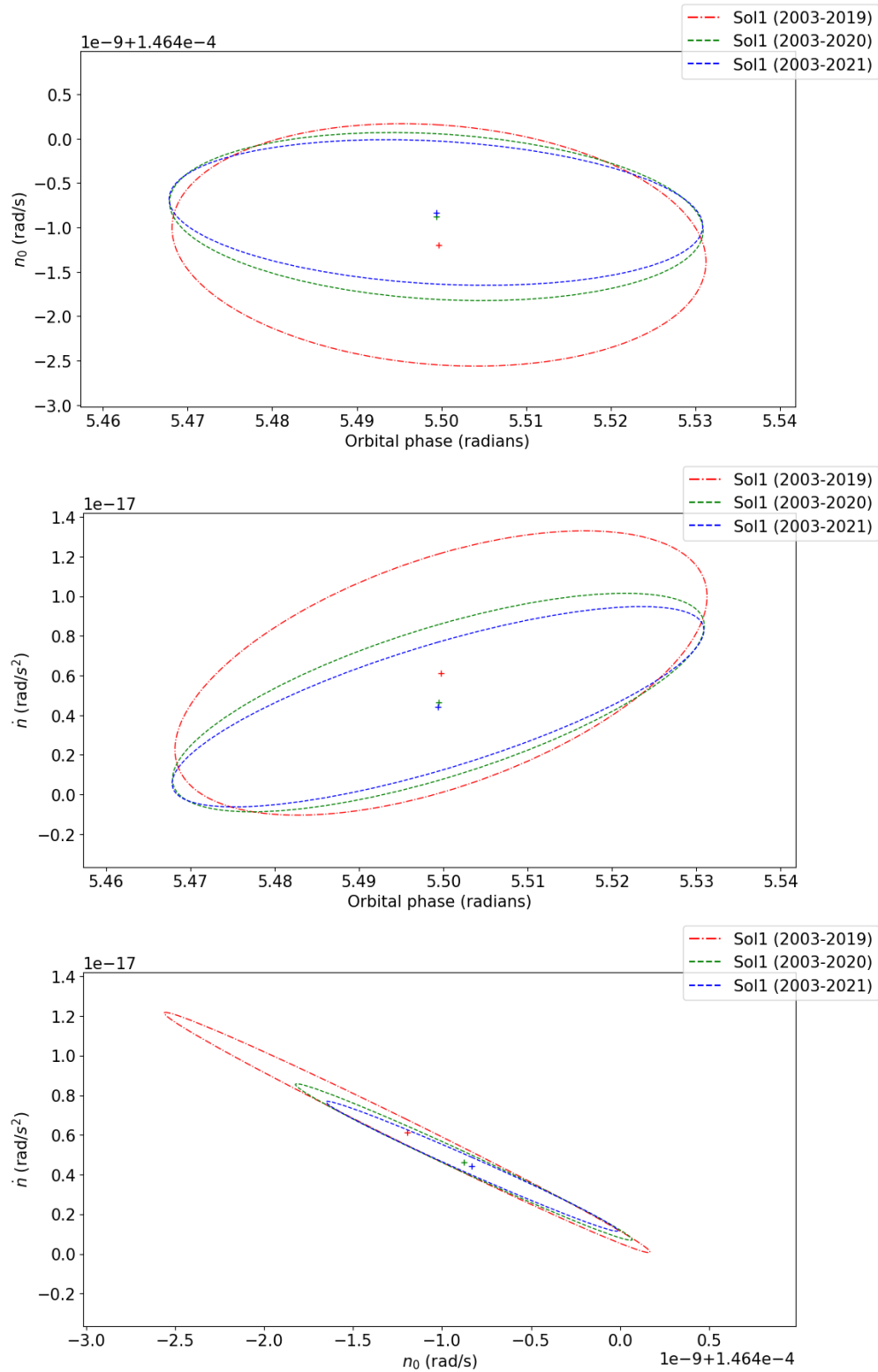


Figure 4: Projections of the best-fit parameters and their 3σ uncertainty regions from the forward prediction test for solution 1 of IOM 392R-20-001. Solutions are at epoch 2003-Nov-20.0 TDB.

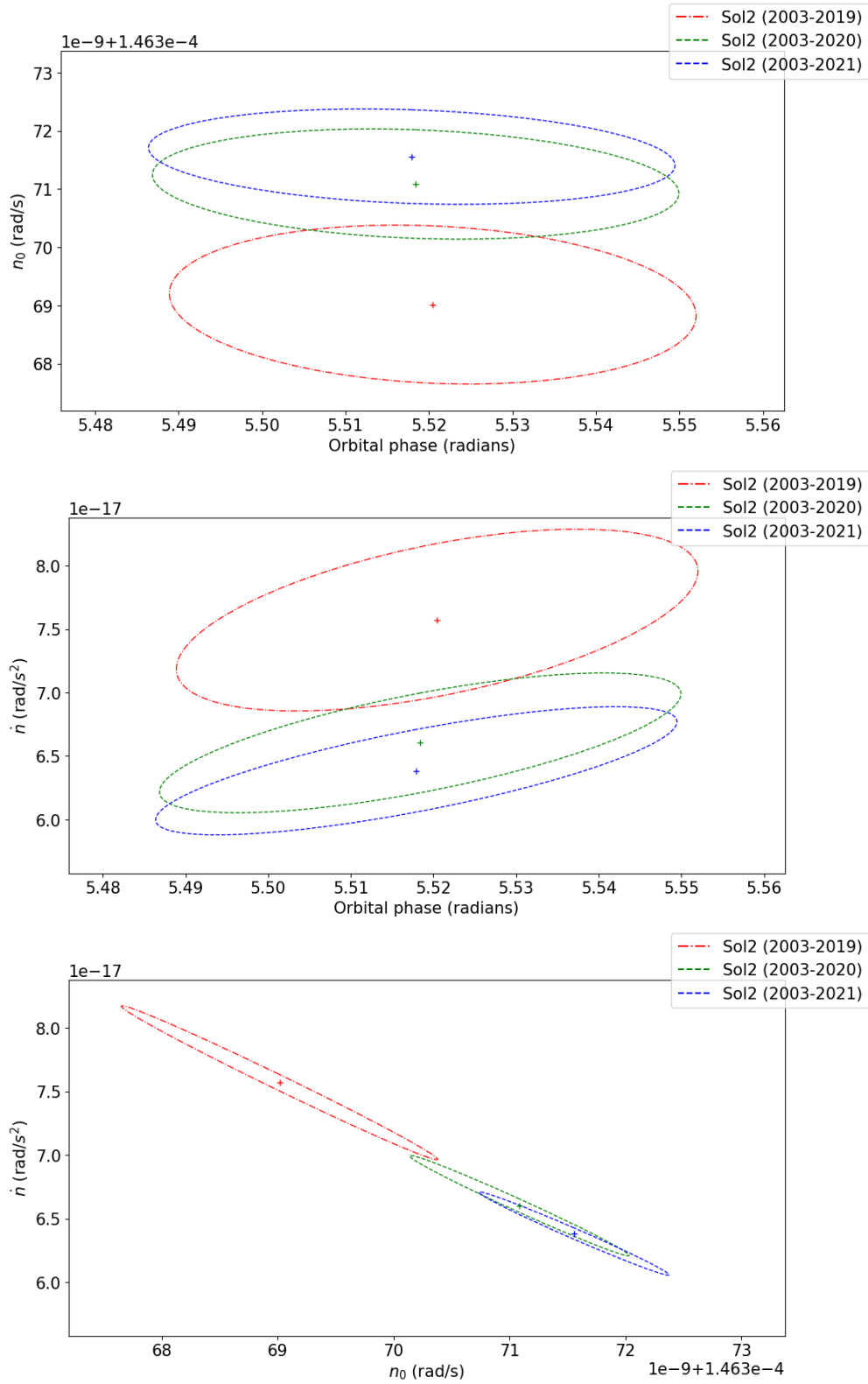


Figure 5: Projections of the best-fit parameters and their 3σ uncertainty regions from the forward prediction test for solution 2 of IOM 392R-20-001. Solutions are at epoch 2003-Nov-20.0 TDB.

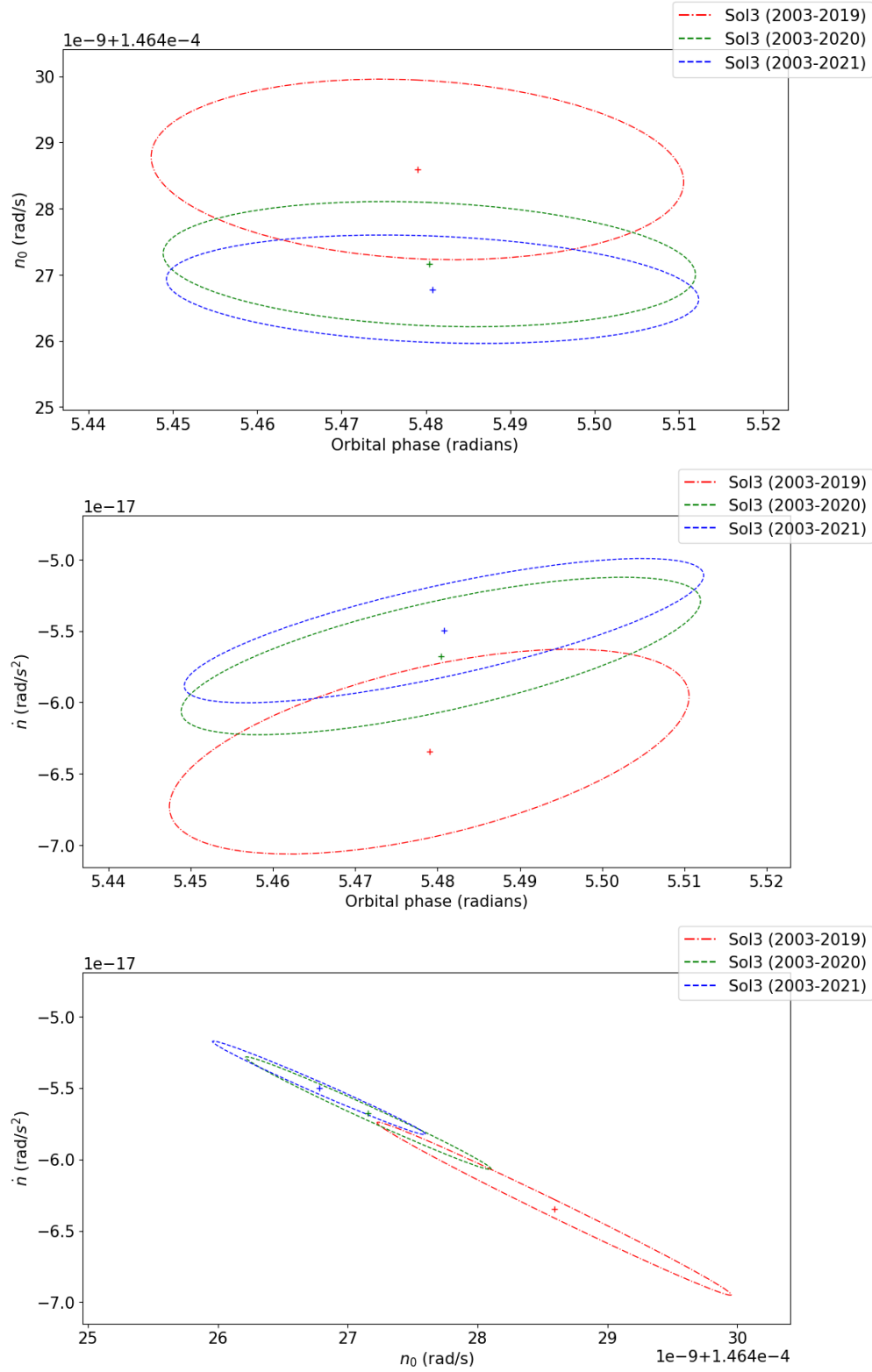


Figure 6: Projections of the best-fit parameters and their 3σ uncertainty regions from the forward prediction test for solution 3 of IOM 392R-20-001. Solutions are at epoch 2003-Nov-20.0 TDB.

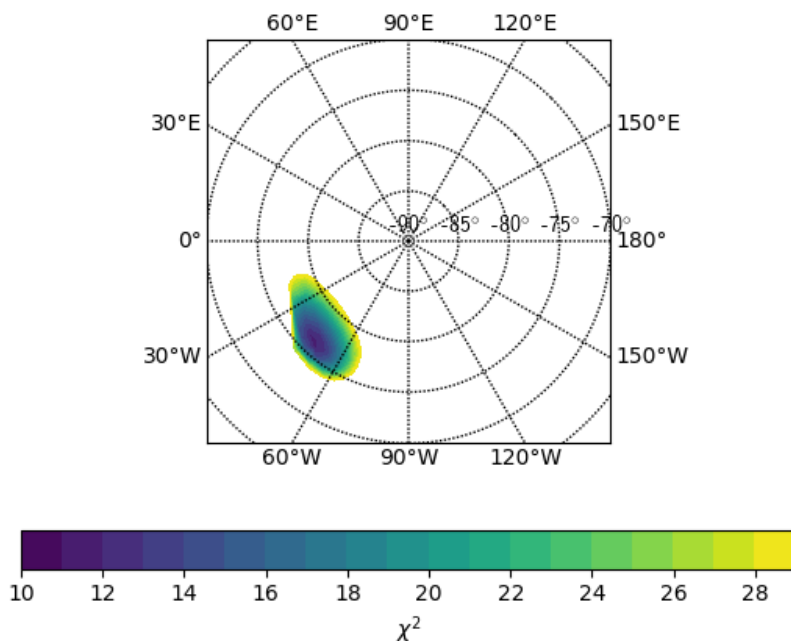


Figure 7: Contour plot of χ^2 as a function of orbit pole, seen from the ecliptic south pole.

orientation. The best-fit orbit pole is at ecliptic $(\lambda, \beta) = (315, -77)^\circ$, which is about 2° from the best-fit pole reported by Scheirich and Pravec (2021) of $(320, -79)^\circ \pm (3.5, 2)^\circ$ (3σ uncertainties). We estimated orbit poles for solutions 2 and 3 using a similar method, but the best-fit χ^2 s were significantly higher than that of solution 1.

Since Scheirich and Pravec (2021) use a more detailed model that fits the entire lightcurve, we adopted their orbit pole of $(320, -79)^\circ$ to generate the nominal Dimorphos orbit solution for delivery to the DART project.

2.3 Best-fit solution

Table 2 shows the best-fit parameters and formal 1σ uncertainties estimated using the adopted orbit pole. Table 3 shows the corresponding covariance. We numbered this solution 101. Figure 8, shows the predicted orbital phase and formal 3σ uncertainty during the planned DART impact for solutions using various observational arc-lengths. The formal 3σ uncertainty using the entire dataset (solution 101) is about 6.6° . Based on tests performed in IOM 392R-20-001, we recommend that the formal uncertainties derived from the covariance matrix in Table 3 be multiplied by 1.3.

The orbital parameters of solution 101 and predicted position of Dimorphos around the time of the DART impact are consistent with those estimated by Scheirich and Pravec (2021) to within 1σ .

Table 2: Best-fit orbital parameters to data from 2003 to 2021 and their formal 1σ uncertainties (solution 101). M_0 , n_0 and \dot{n} were fit. Pole (λ, β) is not estimated and is from Scheirich and Pravec (DART internal report). The osculating period is derived from n_0 . GM_{sys} is the standard gravitational parameter of the system and is derived from the estimated value of n_0 and assumed value of the semimajor axis at epoch. $\chi^2_v = \chi^2 / (n_{\text{obs}} - n_{\text{est}})$ is the reduced χ^2 , where n_{obs} is the number of observations and n_{est} is the number of estimated parameters.

Parameter	Value	1σ uncertainty
M_0 ($^\circ$)	78.9	1.9
Period (h)	11.9216287	0.0000031
n_0 (rad s^{-1})	1.46400235e-04	0.00000038e-4
\dot{n} (rad s^{-2})	4.9e-18	1.1e-18
Epoch (TDB)	2011-08-21.5	
χ^2	20.0	
χ^2_v	0.42	
$(\lambda, \beta)^\circ$	(320, -79) $^\circ$	
GM_{sys} ($\text{m}^3 \text{s}^{-2}$)	37.0362739237411501789	

Table 3: Covariance matrix corresponding to solution 101 in Table 2 at epoch 2011 August 21.5 TDB. Units of the parameters are in radians and seconds.

	M_0	n_0	\dot{n}
M_0	1.13191464e-03	2.32250925e-13	-3.53619250e-20
n_0	2.32250925e-13	1.40712362e-21	-3.95286521e-30
\dot{n}	-3.53619250e-20	-3.95286521e-30	1.19103200e-36

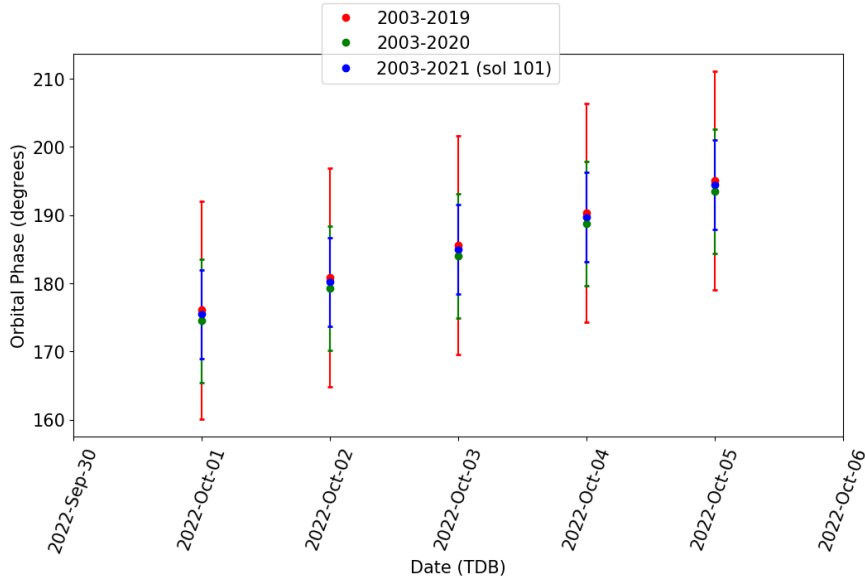


Figure 8: Predicted orbital phase and formal 3σ uncertainties during the planned DART impact using various data-arc lengths.

Delivery

SPICE IDs. We are using a new extended SPICE ID scheme for SPICE kernels delivered in support of the DART mission. This scheme derives the SPICE ID from the asteroid’s IAU number from

$$\text{SPICE ID} = \text{IAU No.} + 20,000,000.$$

This SPICE ID refers generally to the barycenter of a system, including for solitary asteroids. If this number is prepended with a single digit from 1–9 then the ID refers to a specific component of a multi-body system, with ‘9’ being used to designate the primary body. For the Didymos system the following SPICE IDs apply.

SPICE ID	Associated Position
20065803	Didymos system barycenter
120065803	Dimorphos center of mass (secondary body)
920065803	Didymos center of mass (primary body)

Files. The following files and documentation for Dimorphos are available from the JPL Solar System Dynamics (SSD) FTP server

`ftp://ssd.jpl.nasa.gov`

in the directory `pub/eph/small_bodies/dart/`, which will be the base directory for DART file deliveries from SSD. Within the `dart` directory are three sub-directories as follows:

`dart/didymos/` This directory holds the current ephemeris files for the Didymos system barycenter.

`dart/dimorphos/` This directory holds the current ephemeris and related files for Dimorphos:

`dimorphos_s101.bsp` - SPK file containing the ephemeris of Dimorphos (120065803) relative to the primary (920065803) and of 920065803 relative to the Didymos system barycenter (20065803). The latter was computed by assuming a secondary to primary mass ratio of 0.0071 from Naidu et al. (2020).

The time span of the SPK file is from 2000-Jan-01 to 2030-Dec-31. The associated covariance is listed in Table 3. We suggest scaling the formal uncertainties derived from this covariance by a factor of 1.3 in order to capture contributions from unmodeled parameters.

`dimorphos_s101.tpc` - Planetary Constants Kernel (PCK) file that describes the orientation of dimorphos. The PCK file is designed to keep the body-fixed x-axis of Dimorphos oriented towards the system barycenter.

`dart/doc/` This directory includes miscellaneous documentation files.

Acknowledgement

We would like to thank Petr Pravec and Petr Scheirich for suggestions to improve our measurement and modeling methods, as well as for providing the decomposed lightcurves. We would also like to thank Nick Moskowicz for providing decomposed lightcurves from the 2020-2021 observing apparition.

This work was carried out at the Jet Propulsion Laboratory, California Institute of Technology, under a contract with the National Aeronautics and Space Administration (80NM0018D0004).

References

- Acton, C., Bachman, N., Semenov, B., and Wright, E. (2018). A look towards the future in the handling of space science mission geometry. *Planetary and Space Science*, 150:9–12.
- Naidu, S. P., Benner, L. A. M., Brozovic, M., Nolan, M. C., Ostro, S. J., Margot, J. L., Giorgini, J. D., Hirabayashi, T., Scheeres, D. J., Pravec, P., Scheirich, P., Magri, C., and Jao, J. S. (2020). Radar observations and a physical model of binary near-Earth asteroid 65803 Didymos, target of the DART mission. *Icarus*, 348:113777.
- Pravec, P., Scheirich, P., Kušnirák, P., Šarounová, L., Mottola, S., Hahn, G., Brown, P., Esquerdo, G., Kaiser, N., Krzeminski, Z., Pray, D. P., Warner, B. D., Harris, A. W., Nolan, M. C., Howell, E. S., Benner, L. A. M., Margot, J. L., Galád, A., Holliday, W., Hicks, M. D., Krugly, Y. N., Tholen, D., Whiteley, R., Marchis, F., DeGraff, D. R., Grauer, A., Larson, S., Velichko, F. P., Cooney, W. R., Stephens, R., Zhu, J., Kirsch, K., Dyvig, R., Snyder, L., Reddy, V., Moore, S., Gajdoš, Š., Világi, J., Masi, G., Higgins, D., Funkhouser, G., Knight, B., Slivan, S., Behrend, R., Grenon, M., Burki, G., Roy, R., Demeautis, C., Matter, D., Waelchli, N., Revaz, Y., Klotz, A., Rieugn e, M., Thierry, P., Cotrez, V., Brunetto, L., and Kober, G. (2006). Photometric survey of binary near-Earth asteroids. *Icarus*, 181(1):63–93.
- Scheirich, P. and Pravec, P. (2021). Results from modeling of photometric data of Didymos (2003 – 2021a). Technical report, DART internal report.

 2021. California Institute of Technology. Government sponsorship acknowledged.